Reversible tuning of the collapsed tetragonal phase transition in CaFe$_2$As$_2$ by separate control of chemical pressure and electron doping

K. Zhao,[1] C. Stingl,[1] R. S. Manna,[1] C. Q. Jin,[2,3] and P. Gegenwart[1]

[1]*Experimentalphysik VI, Center for Electronic Correlations and Magnetism, University of Augsburg, 86159 Augsburg, Germany*
[2]*Beijing National Laboratory for Condensed Matter Physics and Institute of Physics, Chinese Academy of Sciences, Beijing 100190, China*
[3]*Collaborative Innovation Center of Quantum Matter, Beijing, China*

Single crystals of Ca(Fe$_{1-x}$Ru$_x$)$_2$As$_2$ ($0 \leqslant x \leqslant 0.065$) and Ca$_{1-y}La_y$(Fe$_{0.973}Ru_{0.027}$)$_2As_2$ ($0 \leqslant y \leqslant 0.2$) have been synthesized and studied with respect to their structural, electronic, and magnetic properties. The partial substitution of Fe by Ru induces a decrease of the c-axis constant leading for $x \leqslant 0.023$ to a suppression of the coupled magnetic and structural (tetragonal to orthorhombic) transitions. At $x_{cr} = 0.023$ a first-order transition to a collapsed tetragonal (CT) phase is found, which behaves like a Fermi liquid and which is stabilized by further increase of x. The absence of superconductivity near x_{cr} is consistent with truly hydrostatic pressure experiments on undoped CaFe$_2$As$_2$. Starting in the CT regime at $x = 0.027$, we investigate the additional effect of electron doping by partial replacement of Ca by La. Most remarkably, with increasing y the CT phase transition is destabilized and the system is tuned back into a tetragonal ground state at $y \geqslant 0.08$. This effect is ascribed to a weakening of interlayer As-As bonds by electron doping. Upon further electron doping filamentary superconductivity with T_c of 41 K at $y = 0.2$ is observed.

I. INTRODUCTION

Since the discovery of the iron-arsenide-based superconductor LaO$_{1-x}$F$_x$FeAs with superconducting transition temperature $T_c = 26$ K [1], a series of "1111," "122," "111," or "11" type pnictide superconductors, together with chalcogenide superconductors, were synthesized [2–9]. The AFe$_2$As$_2$ (A = Ca, Sr, Ba, or Eu) 122 parent compounds display structural and magnetic transitions from a high-temperature tetragonal (Tet) paramagnetic to a low-temperature orthorhombic (Ort) magnetic phase. Pressure and chemical doping have similar effects on tuning the electronic structure and phase diagram of AFe$_2$As$_2$ systems [10]. CaFe$_2$As$_2$ is special among the 122 materials as, due to its reduced unit cell volume and c-lattice parameter, it is very close to the collapsed tetragonal (CT) phase. At ambient conditions, CaFe$_2$As$_2$ displays a first-order combined Tet to Ort and magnetic transition at 165 K [11,12]. It is extremely sensitive to the pressure conditions, including both the pressure cell type and the pressure transmitting medium [13]. CaFe$_2$As$_2$ has been tuned to a collapsed tetragonal phase at pressures above 0.35 GPa at 50 K [14,15], with a pressure-induced superconducting phase between 0.23 and 0.86 GPa detected in a nonmagnetic, piston-cylinder-type, Be-Cu pressure cell [16]. However, no superconductivity is observed for single-crystal CaFe$_2$As$_2$ under truly hydrostatic conditions in a helium gas pressure system [17].

The CT phase has also been induced by strain [18] or chemical substitution in CaFe$_2$(As$_{1-x}$P$_x$)$_2$ [19], Ca(Fe$_{1-x}$Rh$_x$)$_2$As$_2$ [20], and Ca$_{1-x}$Pr$_x$Fe$_2$As$_2$ [21]. In the former two materials, the CT phase transition results in large c-parameter changes and leads to a strong change of the electrical resistivity and the magnetic properties, which indicate ordinary Fermi liquid behavior. For Ca$_{1-x}$Pr$_x$Fe$_2$As$_2$ the electronic structure within the CT phase is different compared to CaFe$_2$As$_2$ under pressure (or chemical pressure), likely due to the charge carrier doping effect by Pr^{3+} [22–24]. Because of its significantly smaller ionic radius compared to Ca, Pr substitution introduces both chemical pressure and electron doping [21]. It is therefore

highly interesting to disentangle the influence of these two effects.

Previously, it has been demonstrated for Ba(Fe$_{1-x}$Ru$_x$)$_2$As$_2$ that the isovalent substitution of Fe by Ru effectively acts as chemical pressure. Although Ru is bigger than Fe, the c parameter and c/a ratio shrink in this series and the phase diagram versus x could be scaled by pressure: both 3 GPa of applied pressure and 10% Ru substitution for Fe affect the phase diagram in a similar manner [25,26]. However, it appears that up to now the effect of Ru doping in Ca(Fe$_{1-x}$Ru$_x$)$_2$As$_2$ has not been investigated. We therefore decided to first investigate the effect of chemical pressure in Ca(Fe$_{1-x}$Ru$_x$)$_2$As$_2$ and subsequently to study the influence of electron doping by codoping of divalent Ca by trivalent La in Ca$_{1-y}$La$_y$(Fe$_{1-x}$Ru$_x$)$_2$As$_2$ for selected chemical pressure. Note that, due to the similar ionic radii of La and Ca, the electron doping by La substitution does not induce additional chemical pressure. We can therefore systematically tune the CaFe$_2$As$_2$ ground state by chemical pressure into the CT phase and subsequently investigate the influence of electron doping within this state. Most interestingly, electron doping destabilizes the CT phase and allows tuning of the ground state back towards the Tet phase. We also demonstrate the emergence of superconductivity with T_c above 40 K when the CT phase is suppressed by electron doping.

After a short summary of experimental details we first discuss the temperature-composition (T-x) phase diagram of Ca(Fe$_{1-x}$Ru$_x$)$_2$As$_2$ based on structural, magnetic, and transport measurements. We establish the emergence of the CT ground state at $x > 0.023$ and further systematically investigate the influence of electron doping in Ca$_{1-y}$La$_y$(Fe$_{0.973}$Ru$_{0.027}$)$_2$As$_2$, before the paper ends with a summary of the results.

II. EXPERIMENT

High-quality single crystals of Ca(Fe$_{1-x}$Ru$_x$)$_2$As$_2$ were grown using the FeAs flux method. Mixtures with the ratio

of $Ca:Fe:Ru:As = 1:4-4x:4x:4$ were placed in alumina crucibles and sealed in Ta crucibles under argon atmosphere, heated to 1180 °C for 15 h and slowly cooled to 950 °C at a rate of 3 K/h before cooling to room temperature at a rate of 120 K/h. Mechanically isolated from the flux, platelike crystals were obtained with typical size $2 \times 2 \times 0.1$ mm^3. A similar method was used for the growth of single crystals of $Ca_{1-y}La_y(Fe_{0.973}Ru_{0.027})_2As_2$ with La content up to $y = 0.2$.

Previously the effect of postgrowth annealing on air-quenched-grown single crystals of $CaFe_2As_2$ [18] and $Ca(Fe_{1-x}Co_x)_2As_2$ [27,28] has been reported. Rapidly quenched crystals have substantial internal strain which has a drastic influence on the physical properties. For our growth procedure with slow cooling, only very little strain with negligible effect on the phase diagram is evidenced by the perfect similarity of the our phase diagram for $Ca(Fe_{1-x}Ru_x)_2As_2$ with that of $CaFe_2As_2$ under truly hydrostatic pressure [17].

The actual compositions x and y of the substitutions have been determined by energy-dispersive x-ray (EDX) fluorescence spectrometer measurements. Three crystals were chosen for each concentration for the EDX measurements. Each crystal was investigated on two or three different positions. The crystals were found to be homogeneous with less than 5% relative variation of the actual compositions. All compositions listed in this paper are actual compositions, which differ from the nominal (starting) compositions. All single crystals were characterized via x-ray diffraction with a Philips X'pert diffractometer using Cu $K\alpha_1$ radiation. The dc magnetic susceptibility was characterized using a superconducting quantum interference device magnetometer (Quantum Design, Inc.), whereas the electrical resistivity was measured using the standard four-probe method with a commercial (Quantum Design, Inc.) physical property measurement system (PPMS). The c-axis thermal expansion was measured by utilizing a high-resolution capacitive dilatometer in the PPMS [29].

III. RESULTS AND DISCUSSION

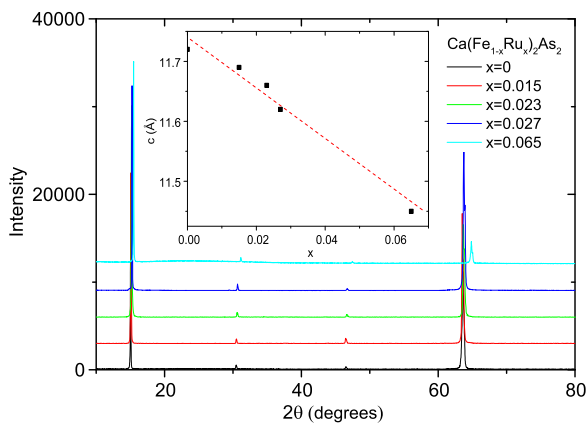Figure 1 shows the x-ray diffraction patterns of single-crystalline $Ca(Fe_{1-x}Ru_x)_2As_2$ for $x = 0$, 0.015, 0.023, 0.027,

FIG. 1. (Color online) X-ray diffraction pattern of single-crystal $Ca(Fe_{1-x}Ru_x)_2As_2$ for $x = 0$, 0.015, 0.023, 0.027, and 0.065, respectively. Inset: the c-axis lattice parameters derived from the (002) peak of the diffraction patterns.
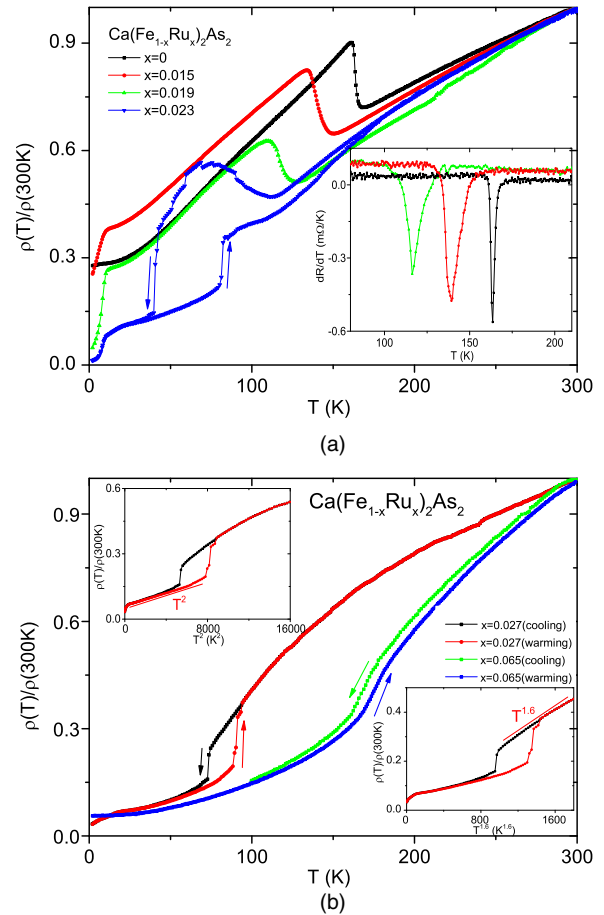

FIG. 2. (Color online) (a) Temperature-dependent normalized electrical resistivity of single-crystal $Ca(Fe_{1-x}Ru_x)_2As_2$ ($0 \leqslant x \leqslant 0.023$), during cooling and warming conditions for $x = 0.023$. (Lower inset) $dR(T)/dT$ versus T from 80 to 210 K for $x = 0$, 0.015, and 0.019, respectively. (b) Temperature-dependent normalized electrical resistivity of single-crystal $Ca(Fe_{1-x}Ru_x)_2As_2$ ($0.023 \leqslant x \leqslant 0.065$). (Lower inset) ρ vs $T^{1.6}$ for $Ca(Fe_{1-x}Ru_x)_2As_2$ with $x = 0.027$. (Upper inset) ρ vs T^2 for $Ca(Fe_{1-x}Ru_x)_2As_2$ with $x = 0.027$.

and 0.065, respectively. Only (00n) peaks are observed, indicating the perfect orientation in the single crystals. Increasing the Ru doping level moves the peaks to higher diffraction angles. This corresponds to a shrinking of the c axis as indicated in the inset of Fig. 1 and expected from previous studies of $Ba(Fe_{1-x}Ru_x)_2As_2$ [30] and $Ca(Fe_{1-x}Rh_x)_2As_2$ [20].

Figure 2(a) displays the normalized electrical resistivity of single-crystalline $Ca(Fe_{1-x}Ru_x)_2As_2$ ($0 \leqslant x \leqslant 0.023$) from 2 to 300 K. For $x = 0.023$ a hysteresis between cooling and warming conditions is found. The resistive anomaly at 163 K for pure $CaFe_2As_2$ is associated with the coupled structural (Tet to Ort) and magnetic phase transitions. As Ru doping increases, the transition temperature is suppressed monotonically and the change of the resistivity at the transition evolves from a sharp feature in pure $CaFe_2As_2$ to a broadened signature, similar to that found for $Ba(Fe_{1-x}Ru_x)_2As_2$ [30]. As shown in the inset of Fig. 2(a), the transition temperature has been determined by the peak position in $d(R(T))/dT$ to be 139 and 116 K for $x = 0.015$ and 0.019, respectively. Note that the single peaks indicate joint structural and magnetic transitions.

In contrast to the case of electron doping in $Ca(Fe_{1-x}Co_x)_2As_2$ [31], the coupling of magnetic and structural transitions upon doping has previously been found in $Ba(Fe_{1-x}Ru_x)_2As_2$ and $(Ba_{1-x}K_x)Fe_2As_2$ [32,33]. As the temperature decreases, the $x = 0.023$ single crystal changes from the Tet phase to the Ort phase, and finally into the CT phase. The latter transition exhibits a significant hysteresis between cooling (42 K) and warming (82 K) conditions, indicating a first-order transition [17]. The observed resistivity fluctuations between the Ort and CT phase transitions likely reflect the competition of these two orderings upon cooling. Upon warming, due to the large hysteresis, there is no obvious indication of the Ort phase transition in the resistivity data. Furthermore, the resistivity displays a drop near 10 K but does not reach zero.

As shown in Fig. 2(b), with increasing Ru substitution for $0.023 \leqslant x \leqslant 0.065$ the Ort phase transition is completely suppressed and the CT phase is stabilized and shifted towards higher temperatures, i.e., 73 K (90 K) for $x = 0.027$ and 165 K (175 K) for $x = 0.065$ upon cooling (warming). Just as for $CaFe_2(As_{1-x}P_x)_2$ [19] and $Ca(Fe_{1-x}Rh_x)_2As_2$ [20], a change from non-Fermi-liquid- to Fermi-liquid-like electrical resistivity behavior is found in the CT phase for $Ca(Fe_{1-x}Ru_x)_2As_2$. In the lower inset of Fig. 2(b), it is displayed that the $x = 0.027$ sample exhibits non-Fermi-liquid behavior, $\Delta R \propto T^{1.6}$, due to antiferromagnetic (AF) fluctuations in the Tet phase [19,20]. The upper inset indicates Fermi-liquid behavior, $\Delta R \propto T^2$, in the CT phase, as found previously, which could be related to the disappearance of magnetic fluctuations [19,20]. The increase of the CT transition temperature with Ru doping shares similarities with that of $Ca(Fe_{1-x}Rh_x)_2As_2$ [20] and $CaFe_2As_2$ under hydrostatic pressure [17].

Figure 3 shows high-field (5 T) magnetic susceptibility data of $Ca(Fe_{1-x}Ru_x)_2As_2$ single crystals for $x = 0$, 0.015, and 0.027 for $H//ab$. In the high-temperature Tet phase, an approximately linear relationship is observed in the temperature dependence of the magnetic susceptibility in all crystals. The $\chi(T)$ data for $x = 0$ and 0.015 show clear spin-density-wave (SDW) anomalies at transition temperatures 163 and 137 K, consistent with the values determined from the electrical resistivity. For $x = 0.027$, the CT phase transition gives rise to a hysteresis between 75 and 90 K upon cooling and warming,
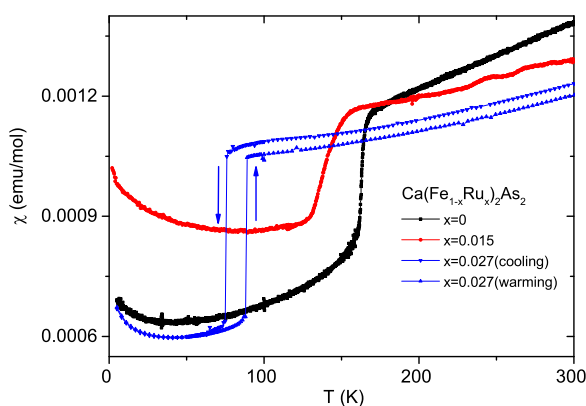

FIG. 3. (Color online) Magnetic susceptibility $\chi(T)$ in a field of 5 T applied parallel to the ab plane of $Ca(Fe_{1-x}Ru_x)_2As_2$ for $x = 0$, 0.015, and 0.027, respectively.
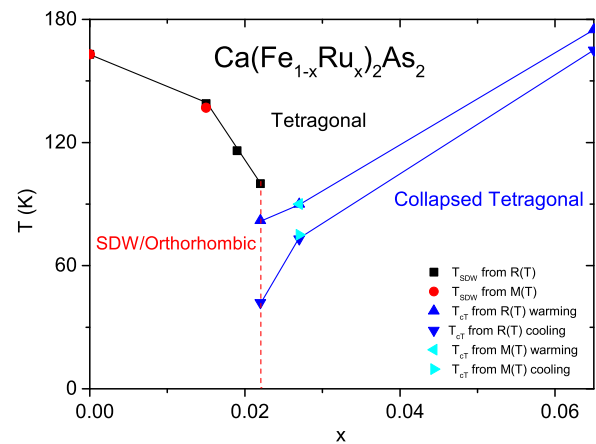

FIG. 4. (Color online) Temperature-composition (T-x) phase diagram of single-crystal $Ca(Fe_{1-x}Ru_x)_2As_2$ ($0 < x < 0.065$). T_{SDW} represents the structural and magnetic transitions. T_{cT} shows the collapsed tetragonal transition temperatures in warming and cooling conditions.

again consistent with the electrical resistivity and previous observations on $CaFe_2(As_{1-x}P_x)_2$ [19], $Ca(Fe_{1-x}Rh_x)_2As_2$ [20], and $(Ca_{1-x}Pr_x)Fe_2As_2$ [21].

Based on these data we have constructed the temperature-composition phase diagram displayed in Fig. 4. At $x = 0.023$ a discontinuous first-order change from the Ort to the CT ground state is observed. With further chemical pressure, the CT phase is stabilized. There is no bulk superconducting regime. The phase diagram resembles that found under truly hydrostatic pressure for $CaFe_2As_2$ [17]. For 0.35 GPa hydrostatic pressure, $CaFe_2As_2$ also changes directly from the Ort phase into the CT phase upon cooling, with a CT transition temperature of 40 K, similar to that found for $x = 0.023$ at ambient pressure. Thus, as in $Ba(Fe_{1-x}Ru_x)_2As_2$, partial Ru substitution of the Fe atoms mainly acts as chemical pressure.

This together with the results of truly hydrostatic pressure experiments [17] indicates that superconductivity in $CaFe_2As_2$ requires either anisotropic strain induced by nonhydrostatic pressure conditions or additional charge carrier doping. This is in contrast to the cases of $BaFe_2As_2$ and $SrFe_2As_2$ [13]. The origin of this difference is, that for $CaFe_2As_2$ under hydrostatic or chemical pressure, the CT ground state appears (in a first-order transition) before the Ort/magnetic ground state is fully suppressed. Compared with isoelectronic Ru substitution, there is an additional electron doping effect in the case of $Ca(Fe_{1-x}Rh_x)_2As_2$ [20]. For the latter series, the Ort/magnetic phase can be suppressed continuously down to low temperatures and a small superconductivity dome appears before the CT phase is entered [20].

In order to disentangle the effect of charge carrier doping from that of chemical pressure, we have chosen $x = 0.027$ with a well-established CT ground state for a series with additional La substitution at the Ca site, which gives rise to electron doping. Figure 5 shows the x-ray diffraction patterns of single-crystalline $Ca_{1-y}La_y(Fe_{0.973}Ru_{0.027})_2As_2$ for $y = 0.04$, 0.06, 0.08, 0.15, and 0.20, respectively. Only (00l) peaks are observed, indicating good quality of the single crystals. From the inset of Fig. 5, the (002) peaks of the
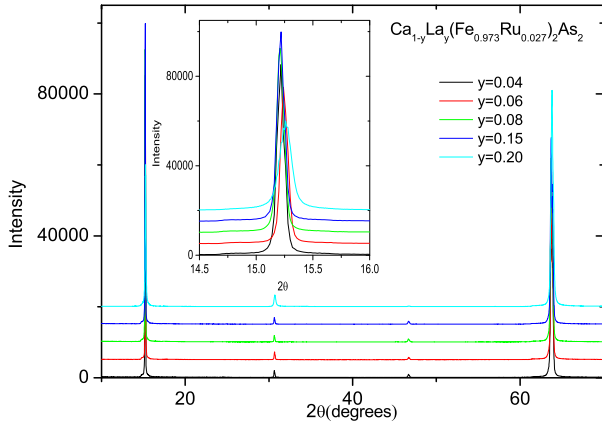
FIG. 5. (Color online) X-ray diffraction pattern of single-crystal $Ca_{1-y}La_y(Fe_{0.973}Ru_{0.027})_2As_2$ for $y = 0.04$, 0.06, 0.08, 0.15, and 0.20, respectively. Inset: enlargement of the (002) peak of the diffraction patterns.

diffraction patterns randomly vary from 15.21° to 15.26°. Concerning the (002) peak of $Ca(Fe_{0.973}Ru_{0.027})_2As_2$ located at 15.24°, these results imply that, with a similar ionic radius as Ca, La doping does not obviously decreases the c axis. Therefore, as for $Ca_{1-x}La_xFe_2As_2$ [21], La substitution in $Ca_{1-y}La_y(Fe_{0.973}Ru_{0.027})_2As_2$ realizes electron doping without additional chemical pressure.

At low La doping, i.e., $y = 0.04$, the electrical resistivity and magnetic susceptibility data [cf. Fig. 6(a) and the lower inset of this figure] are rather similar to those of $y = 0$. The first-order CT phase transition is slightly destabilized and observed at 64 K upon cooling and 76 K during warming. Again Fermi-liquid behavior is found within the CT phase (see the upper inset). Further La doping shifts the CT transition to lower values. As shown in Fig. 6(b) for $y = 0.06$, a hysteresis is still found in the magnetic susceptibility between 43 K (cooling) and 49 K (warming). On the other hand, the signature and hysteresis in the electrical resistivity [inset of Fig. 6(b)] are already very much suppressed, as in $Ca_{1-x}Pr_xFe_2As_2$ for $x = 0.145$ [21]. Altogether the results indicate that La doping in $Ca_{1-y}La_y(Fe_{0.973}Ru_{0.027})_2As_2$ decreases the CT transition temperature, the amplitude of the resistivity jump at the CT transition, and the width of hysteresis.

Indeed, further increase of La doping completely suppresses the CT transition signatures in electrical resistivity and magnetic susceptibility, as shown for $y = 0.08$ in Fig. 6(c). There is a broad kink around 90 K in the magnetic susceptibility in 5 T [see the upper inset of Fig. 6(c)], which probably arises from the competition between the tetragonal and the CT phases. For this concentration two broad drops of the electrical resistivity at 42 K (T_{c1}) and 25 K (T_{c2}), which are easily suppressed by application of a small magnetic field [see the lower inset of Fig. 6(c)] may be associated with incipient superconductivity (not bulk, since neither complete suppression of the resistivity nor significant diamagnetism occurs).

Further enhancement of the La doping ($y = 0.15$) leads to more pronounced superconducting anomalies in the electrical resistivity, which now at T_{c2} approaches zero [lower inset of Fig. 6(d)]. The upper transition (T_{c1}) signature becomes

further enhanced at $y = 0.2$ [Fig. 6(d) main part and upper inset]. The low-field magnetic susceptibility for the latter La concentration $y = 0.2$ also displays a clear diamagnetic response associated with T_{c1} and T_{c2} under both zero-field cooling (ZFC) and field cooling (FC) conditions [Fig. 6(e)], which further evidences superconductivity. Note, however, that the size of the diamagnetic signal is weak, corresponding to a superconducting volume fraction at low temperatures of order 3% only.

It is interesting to note that two superconducting transitions were found in electrical resistivity measurements on $Ca_{1-x}La_xFe_2As_2$ with or without pressure [34,35]. By contrast only one superconductivity transition has been found in $Sr_{1-x}La_xFe_2As_2$ [36] and $Ba_{1-x}La_xFe_2As_2$ epitaxial thin films [37], with the transition temperature around 20 K, comparable with T_{c2} in our system. As in our system, for codoped $(Ca_{1-y}La_y)Fe_2(As_{1-x}P_x)_2$ with $x = 0.06$ and $y = 0.18$ also an incomplete diamagnetic response has been found below T_{c1} of order 40 K [38]. On the other hand for $Ca_{1-x}La_xFe_2As_2$ the upper transition at T_{c1} is not seen in the magnetic susceptibility, indicating that it is only spurious. This comparison implies that Ru doping or chemical pressure stabilizes superconductivity above 40 K in $Ca_{1-x}La_xFe_2As_2$.

Before summarizing the results on the La-doped material in a phase diagram, we provide final evidence for the complete suppression of the CT transition from c-axis thermal expansion (TE) data, obtained upon warming the sample in a capacitive dilatometer. As shown in Fig. 7, the clear length jump associated with the CT transition for $y = 0.06$ is fully suppressed at $y \geqslant 0.08$, for which a smooth variation of the c parameter is found. This proves a critical concentration y_{cr} close to 0.08 for the CT transition in $Ca_{1-y}La_y(Fe_{0.973}Ru_{0.027})_2As_2$.

Figure 8 displays the resulting phase diagram for the $Ca_{1-y}La_y(Fe_{0.973}Ru_{0.027})_2As_2$ series. Clearly with La doping the CT phase can be suppressed completely. It has been discussed previously that the CT transition is driven by an enhancement of the interlayer As-As bonding [39]. Our individual control of chemical pressure and electron doping in $Ca(Fe_{1-x}Ru_x)_2As_2$ and $Ca_{1-y}La_y(Fe_{0.973}Ru_{0.027})_2As_2$ proves that these two parameters have different effects. While chemical pressure could stabilize the presence of interlayer As-As bonding, successive electron doping obviously weakens the bonding, and finally breaks it. So far, there are several examples, mentioned before, of inducing the CT phase for $CaFe_2As_2$-based materials. Here we have shown tuning of the CT phase back into the tetragonal phase.

Our results indicate that electron doping somehow counteracts chemical pressure in $CaFe_2As_2$. For $Ca_{1-x}Pr_xFe_2As_2$ the observed behavior therefore seems to be determined by the combination of both effects. While the CT transition is induced by chemical pressure, simultaneous electron doping decreases the strength of the interlayer As-As bonding and thereby suppresses the resistivity change at the CT transition.

The study of superconductivity has not been the main focus of this work, but we briefly comment on the observed signatures of incipient superconductivity when the CT phase is completely suppressed by electron doping. This suggests that the CT state is detrimental to superconductivity. According to inelastic neutron scattering and nuclear magnetic resonance measurements on strained $CaFe_2As_2$ [40,41], AF spin
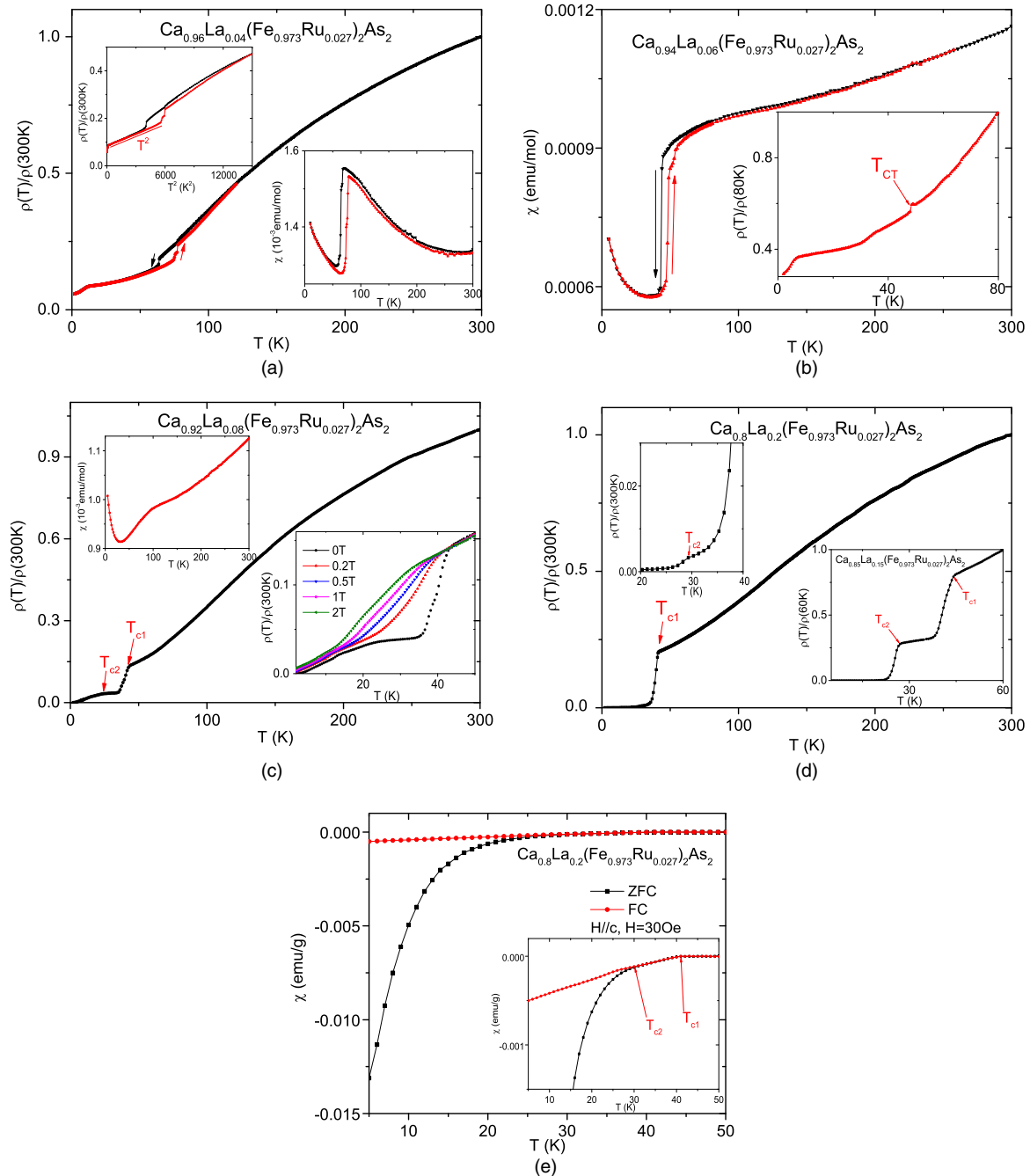
FIG. 6. (Color online) (a) Normalized electrical resistivity for single-crystalline $Ca_{1-y}La_y(Fe_{0.973}Ru_{0.027})_2As_2$ for $y = 0.04$, during cooling and warming. Upper inset: ρ vs T^2 for $x = 0.04$. Lower inset: Magnetic susceptibility $\chi(T)$ for $y = 0.04$, in cooling and warming conditions in $H//ab$ under 5 T. (b)Magnetic susceptibility $\chi(T)$ for $Ca_{1-y}La_y(Fe_{0.973}Ru_{0.027})_2As_2$, with $y = 0.06$, measured at 5 T applied parallel to the ab plane. Lower inset: $\rho(T)/\rho(80\,K)$ of single-crystalline $Ca_{1-y}La_y(Fe_{0.973}Ru_{0.027})_2As_2$ for $y = 0.06$ during warming procedure. (c) Normalized electrical resistivity of single-crystal $Ca_{0.92}La_{0.08}(Fe_{0.973}Ru_{0.027})_2As_2$. Lower inset: $\rho(T)/\rho(300\,K)$ versus T for $y = 0.08$ between 5 and 50 K at several different magnetic fields. Upper inset: $\chi(T)$ for $y = 0.08$ in a field of 5 T applied parallel to the ab direction. (d) Normalized electrical resistivity of single-crystalline $Ca_{0.8}La_{0.2}(Fe_{0.973}Ru_{0.027})_2As_2$. Upper inset: $\rho(T)/\rho(300\,K)$ versus T. Lower inset: $\rho(T)/\rho(60\,K)$ versus T of single-crystal $Ca_{0.85}La_{0.15}(Fe_{0.973}Ru_{0.027})_2As_2$. (e) Magnetic susceptibility $\chi(T)$ of $Ca_{0.8}La_{0.2}(Fe_{0.973}Ru_{0.027})_2As_2$ measured in a field of 30 Oe applied in ZFC (black points) and FC (red points) modes for $H//c$. Lower inset: enlargement of ZFC and FC curves around two superconducting transitions at 41 and 30 K.

fluctuations and electronic correlations are completely absent in the CT state. For the related $Ca_{1-x}Pr_xFe_2As_2$ with $x = 0.14$, recent scanning transmission electron microscopy (STEM) and scanning tunneling microscopy (STM) investigations

found filamentary superconductivity related to an inhomogeneity of the Pr concentration on a nanometer scale [42]. Respectively, incomplete (and possibly filamentary) superconductivity above 40 K in our $Ca_{1-y}La_y(Fe_{0.973}Ru_{0.027})_2As_2$
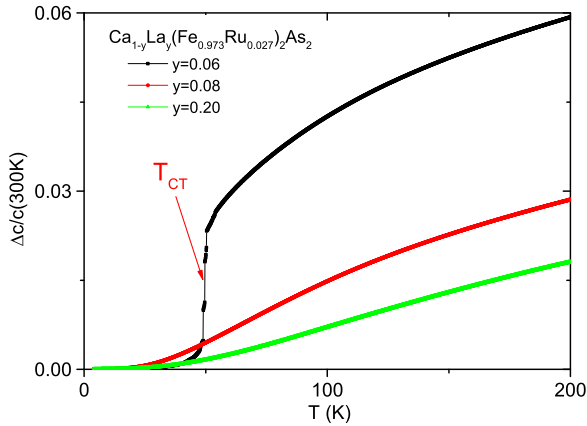
FIG. 7. (Color online) Temperature-dependent c-axis relative length change $[\Delta c/c(300\,\text{K}) = [c(T) - c(300\,\text{K})]/c(300\,\text{K})]$ for single-crystalline $Ca_{1-y}La_y(Fe_{0.973}Ru_{0.027})_2As_2$ for $y = 0.06$, 0.08, and 0.20. All data are obtained upon increasing temperature.

FIG. 8. (Color online) Phase diagram of single-crystal $Ca_{1-y}La_y(Fe_{0.973}Ru_{0.027})_2As_2$ $(0 < y < 0.20)$. T_{cT} represents the collapsed tetragonal transition temperatures in warming and cooling conditions; T_{c1} and T_{c2} denote the two superconducting transitions in the tetragonal phase.

material for $y = 0.2$ may also be related to small local variations of the La and Ru dopants which are impossible to resolve by our microprobe EDX experiments. Importantly, these local inhomogeneities could lead to superconductivity only if the CT phase is fully suppressed. A superconducting gap as large as 30 meV on localized regions indicates the intrinsic nature of the high-temperature superconductivity in this system [42]. Compared to pure $(CaLa)Fe_2As_2$, chemical pressure in $(CaLa)(FeRu)_2As_2$ or $(CaLa)Fe_2(AsP)_2$ drives the material closer to the CT phase. The coinciding enhancement of the diamagnetic response at T_{c1} suggests a stabilization of superconductivity under chemical pressure. This is in accordance with a recent theoretical scenario treating orbital fluctuations related to the CT transition as key ingredient to realize high T_c values in these materials [43].

IV. CONCLUSION

We have demonstrated that the partial substitution of Fe by Ru in $Ca(Fe_{1-x}Ru_x)_2As_2$ acts as chemical pressure. Near $x_{cr} = 0.023$ a discontinuous transition between the AF

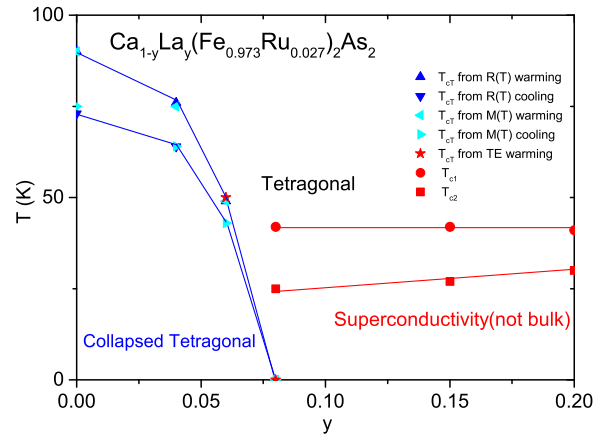Ort ground state and the CT phase with Fermi liquid properties without any superconducting dome was found. Starting within the CT state additional electron doping in $Ca_{1-y}La_y(Fe_{0.973}Ru_{0.027})_2As_2$ substantially weakens the interlayer As-As bonding and tunes the ground state back into the Tet phase. Superconductivity appears within the Tet phase only after complete suppression of the CT phase. This highlights the importance of AF spin fluctuations and electronic correlations to the superconductivity in iron pnictide materials. Chemical pressure in $Ca_{1-x}La_xFe_2As_2$ enhances local superconductivity above 40 K.

[1] Y. Kamihara, T. Watanabe, M. Hirano, and H. Hosono, J. Am. Chem. Soc. **130**, 3296 (2008).

[2] X. H. Chen, T. Wu, G. Wu, R. H. Liu, H. Chen, and D. F. Fang, Nature (London) **453**, 761 (2008).

[3] G. F. Chen, Z. Li, D. Wu, G. Li, W. Z. Hu, J. Dong, P. Zheng, J. L. Luo, and N. L. Wang, Phys. Rev. Lett. **100**, 247002 (2008).

[4] Z.-A Ren, J. Yang, W. Lu, W. Yi, X.-L Shen, Z.-G Li, G.-C Che, X.-L Dong, L.-L Sun, F. Zhou, and Z.-X Zhao, Europhys. Lett. **82**, 57002 (2008).

[5] H. H. Wen, G. Mu, L. Fang, H. Yang, and X. Y. Zhu, Europhys. Lett. **82**, 17009 (2008).

[6] M. Rotter, M. Tegel, and D. Johrendt, Phys. Rev. Lett. **101**, 107006 (2008).

[7] H. S. Jeevan, Z. Hossain, Deepa Kasinathan, H. Rosner, C. Geibel, and P. Gegenwart, Phys. Rev. B **78**, 092406 (2008).

[8] X. C.Wang, Q. Q. Liu, Y. X. Lv, W. B. Gao, L. X.Yang, R. C. Yu, F. Y.Li, and C. Q. Jin, Solid State Commun. **148**, 538 (2008).

[9] F.-C. Hsu, J.-Y. Luo, K.-W. Yeh, T.-K. Chen, T.-W. Huang, P. M. Wu, Y.-C. Lee, Y.-L. Huang, Y.-Y. Chu, D.-C. Yan, and M.-K. Wu, Proc. Natl. Acad. Sci. USA **105**, 14262 (2008).

[10] Simon A. J. Kimber, Andreas Kreyssig, Yu-Zhong Zhang, Harald O. Jeschke, Roser Valentí, Fabiano Yokaichiya, Estelle Colombier, Jiaqiang Yan, Thomas C. Hansen, Tapan Chatterji, Robert J. McQueeney, Paul C. Canfield, Alan I. Goldman, and Dimitri N. Argyriou, Nat. Mater. **8**, 471 (2009).

[11] N. Ni, S. Nandi, A. Kreyssig, A. I. Goldman, E. D. Mun, S. L. Bud'ko, and P. C. Canfield, Phys. Rev. B **78**, 014523 (2008).

[12] F. Ronning, T. Klimczuk, E. D. Bauer, H. Volz, and J. D. Thompson, J. Phys.: Condens. Matter **20**, 322201 (2008).

[13] Johnpierre Paglione and Richard L. Greene, Nat. Phys. **6**, 645 (2010).

[14] A. Kreyssig, M. A. Green, Y. Lee, G. D. Samolyuk, P. Zajde, J. W. Lynn, S. L. Bud'ko, M. S. Torikachvili, N. Ni, S. Nandi, J. B. Leão, S. J. Poulton, D. N. Argyriou, B. N. Harmon, R. J. McQueeney, P. C. Canfield, and A. I. Goldman, Phys. Rev. B **78**, 184517 (2008).

[15] A. I. Goldman, A. Kreyssig, K. Prokeš, D. K. Pratt, D. N. Argyriou, J. W. Lynn, S. Nandi, S. A. J. Kimber, Y. Chen, Y. B. Lee, G. Samolyuk, J. B. Leão, S. J. Poulton, S. L. Bud'ko, N. Ni, P. C. Canfield, B. N. Harmon, and R. J. McQueeney, Phys. Rev. B **79**, 024513 (2009).

[16] Milton S. Torikachvili, Sergey L. Bud'ko, Ni Ni, and P. C. Canfield, Phys. Rev. Lett. **101**, 057006 (2008).

[17] W. Yu, A. A. Aczel, T. J. Williams, S. L. Bud'ko, N. Ni, P. C. Canfield, and G. M. Luke, Phys. Rev. B **79**, 020511(R) (2009).

[18] S. Ran, S. L. Bud'ko, D. K. Pratt, A. Kreyssig, M. G. Kim, M. J. Kramer, D. H. Ryan, W. N. Rowan-Weetaluktuk, Y. Furukawa, B. Roy, A. I. Goldman, and P. C. Canfield, Phys. Rev. B **83**, 144517 (2011).

[19] S. Kasahara, T. Shibauchi, K. Hashimoto, Y. Nakai, H. Ikeda, T. Terashima, and Y. Matsuda, Phys. Rev. B **83**, 060505 (2011).

[20] Masataka Danura, Kazutaka Kudo, Yoshihiro Oshiro, Shingo Araki, Tatsuo C. Kobayashi, and Minoru Nohara, J. Phys. Soc. Jpn. **80**, 103701 (2011).

[21] S. R. Saha, N. P. Butch, T. Drye, J. Magill, S. Ziemak, K. Kirshenbaum, P. Y. Zavalij, J. W. Lynn, and J. Paglione, Phys. Rev. B. **85**, 024525 (2012).

[22] R. S. Dhaka, Rui Jiang, S. Ran, S. L. Bud'ko, P. C. Canfield, B. N. Harmon, Adam Kaminski, Milan Tomić, and Roser Valentí, and Yongbin Lee, Phys. Rev. B. **89**, 020511 (2014).

[23] K. Tsubota, T. Wakita, H. Nagao, C. Hiramatsu, T. Ishiga, M. Sunagawa, K. Ono, H. Kumigashira, M. Danura, K. Kudo, M. Nohara, Y. Muraoka, and T. Yokoya, J. Phys. Soc. Jpn. **82**, 073705 (2013).

[24] D. F. Xu, D. W. Shen, J. Jiang, Z. R. Ye, X. Liu, X. H. Niu, H. C. Xu, Y. J. Yan, T. Zhang, B. P. Xie, and D. L. Feng, Phys. Rev. B. **90**, 214519 (2014),

[25] S. K. Kim, M. S. Torikachvili, E. Colombier, A. Thaler, S. L. Bud'ko, and P. C. Canfield, Phys. Rev. B **84**, 134525 (2011).

[26] R. S. Dhaka, Chang Liu, R. M. Fernandes, Rui Jiang, C. P. Strehlow, Takeshi Kondo, A. Thaler, Jörg Schmalian, S. L. Bud'ko, P. C. Canfield, and Adam Kaminski, Phys. Rev. Lett. **107**, 267002 (2011).

[27] S. Ran, S. L. Bud'ko, W. E. Straszheim, J. Soh, M. G. Kim, A. Kreyssig, A. I. Goldman, and P. C. Canfield, Phys. Rev. B **85**, 224528 (2012).

[28] E. Gati, S. Köhler, D. Guterding, B. Wolf, S. Knöner, S. Ran, S. L. Bud'ko, P. C. Canfield, and M. Lang, Phys. Rev. B **86**, 220511 (2012).

[29] R. Küchler, T. Bauer, M. Brando, and F. Steglich, Rev. Sci. Instrum. **83**, 095102 (2012).

[30] A. Thaler, N. Ni, A. Kracher, J. Q. Yan, S. L. Bud'ko, and P. C. Canfield, Phys. Rev. B **82**, 014534 (2010).

[31] L. Harnagea, S. Singh, G. Friemel, N. Leps, D. Bombor, M. Abdel-Hafiez, A. U. B. Wolter, C. Hess, R. Klingeler, G. Behr, S. Wurmehl, and B. Büchner, Phys. Rev. B **83**, 094523 (2011).

[32] M. G. Kim, D. K. Pratt, G. E. Rustan, W. Tian, J. L. Zarestky, A. Thaler, S. L. Bud'ko, P. C. Canfield, R. J. McQueeney, A. Kreyssig, and A. I. Goldman, Phys. Rev. B **83**, 054514 (2011).

[33] Bing Shen, Huan Yang, Zhao-Sheng Wang, Fei Han, Bin Zeng, Lei Shan, Cong Ren, and Hai-Hu Wen, Phys. Rev. B **84**, 184512 (2011).

[34] Y. Sun, W. Zhou, L. J. Cui, J. C. Zhuang, Y. Ding, F. F. Yuan, J. Bai, and Z. X. Shi, AIP Adv. **3**, 102120 (2013).

[35] Shanta R. Saha, T. Drye, S. K. Goh, L. E. Klintberg, J. M. Silver, F. M. Grosche, M. Sutherland, T. J. S. Munsie, G. M. Luke, D. K. Pratt, J. W. Lynn, and J. Paglione, Phys. Rev. B **89**, 134516 (2014).

[36] Yoshinori Muraba, Satoru Matsuishi, Sung-Wng Kim, Toshiyuki Atou, Osamu Fukunaga, and Hideo Hosono, Phys. Rev. B **82**, 180512 (2010).

[37] Takayoshi Katase, Soshi Iimura, Hidenori Hiramatsu, Toshio Kamiya, and Hideo Hosono, Phys. Rev. B **85**, 140516 (2012).

[38] Kazutaka Kudo, Keita Iba, Masaya Takasuga, Yutaka Kitahama, Jun-ichi Matsumura, Masataka Danura, Yoshio Nogami, and Minoru Nohara, Sci. Rep. **3**, 1478 (2013).

[39] J. R. Jeffries, N. P. Butch, K. Kirshenbaum, S. R. Saha, G. Samudrala, S. T. Weir, Y. K. Vohra, and J. Paglione, Phys. Rev. B **85**, 184501 (2012).

[40] J. H. Soh, G. S. Tucker, D. K. Pratt, D. L. Abernathy, M. B. Stone, S. Ran, S. L. Bud'ko, P. C. Canfield, A. Kreyssig, R. J. McQueeney, and A. I. Goldman, Phys. Rev. Lett. **111**, 227002 (2013).

[41] Y. Furukawa, B. Roy, S. Ran, S. L. Bud'ko, and P. C. Canfield, Phys. Rev. B **89**, 121109 (2014).

[42] Krzysztof Gofryk, Minghu Pan, Claudia Cantoni, Bayrammurad Saparov, Jonathan E. Mitchell, and Athena S. Sefat, Phys. Rev. Lett. **112**, 047005 (2014).

[43] Seiichiro Onari, Youichi Yamakawa, and Hiroshi Kontani, Phys. Rev. Lett. **112**, 187001 (2014).